

Thermal reaction processes in a relativistic QED plasma drop

Inga Kuznetsova, Dieter Habs and Johann Rafelski

Department of Physics, University of Arizona, Tucson, Arizona, 85721, USA and

*Department für Physik der Ludwig-Maximilians-Universität München und
Maier-Leibnitz-Laboratorium, Am Coulombwall 1, 85748 Garching, Germany*

(Dated: October, 30, 2009)

The equilibrium size and temperature limits of thermally and chemically equilibrated $e^+e^-\gamma$ plasma drops are investigated at a given energy content. For a plasma to be equilibrated it must be opaque to electron and photon interactions. The opaqueness condition is determined by comparing plasma size with the mean free electron and photon paths. We calculate those paths using thermal Lorentz-invariant reaction rates for pair production and electron (positron) and photon scattering. The range of the corresponding plasma temperature and size is evaluated numerically. Considering the energy and size we find that the opaque and equilibrated plasma drop may be experimentally attainable.

PACS numbers: 12.20.Ds, 52.27.Ny, 52.25.Fi, 52.38.Ph

I. INTRODUCTION

In [1] we considered relativistic EP³ (e^- , e^+ , γ plasma, **electron, positron photon plasma**) in equilibrium and have studied heavy (muon, pion) particle production rates. Here we extend considerably these methods and study the production and equilibration of the components e^- , e^+ , γ of the EP³ plasma in order to explore the constraints on how such a plasma can be formed, and when it falls apart into free-streaming constituents (freeze-out condition). We evaluate constraints arising from the requirement that a plasma drop ought to be opaque to constituent particle scattering, and include in this consideration the constraint on size and temperature arising from laser pulse energy available to form the plasma. Furthermore, we can determine under what conditions the plasma drop will not only reach thermal (spectral) but also chemical (yield of particles) equilibrium.

In laboratory experiments involving, e.g. ultra intense laser pulses to form strong fields, electron-positron pairs are produced; for review see [2–4]. They rescatter or annihilate and produce hard photons. In a large enough domain the e^+e^- pairs and hard photons γ will equilibrate thermally and chemically. This kinetic equilibration process cannot be resolved in the general study we present here. Instead, we focus our attention on the properties of the $e^+e^-\gamma$ plasma drop near equilibrium in its final evolution stage. We are assuming EP³ was formed in the vacuum state (particle-antiparticle symmetry) and keeping the total zero spin.

In laboratory experiments an initially dense plasma fireball with radius R_{pl} will dilute, expanding at plasma speed of “sound”, nearly speed of light. The lifespan in a fast expanding plasma drop is

$$\tau_{pl} \simeq \frac{\sqrt{3}}{c} R_{pl}.$$

We consider the plasma drop of finite size. However we neglect the energy loss from the radiation of photons from the plasma surface. We assume that if a plasma is opaque

then the energy loss from a surface is insignificant during the plasma lifespan, which is defined by the laser pulse duration. If plasma is nonopaque, then energy loss occurs from the whole plasma volume, signaling the end of equilibrium and onset of transport regime not addressed here.

There are three different conditions which we can track in the plasma state which are usually passed in sequence in time:

1. At highest density (i.e. temperature T) we reach particle yield chemical equilibrium. This is the condition when the e^+e^- -pair annihilation into and production by photons occur at equal rate.
2. At an intermediate density many scattering processes can occur, but not as many as needed to maintain chemical equilibrium. That is the opaqueness domain.
At this time also most photons will leave the plasma free-streaming
3. At yet a lower density, freeze-out of e^+ , e^- occurs; that is, these particles will leave the plasma without further rescattering.

Let us look at how these conditions are obtained, in reverse order: for the particle freeze-out (free-streaming) condition we consider

$$L_i \simeq R_{pl}, \quad \text{free - streaming.} \quad (1)$$

Here we use the thermal free path L_i , $i = e^-, e^+, \gamma$ which is computed below, and compare it to the plasma radius R_{pl} . For plasma to be opaque we require

$$L_i \leq \frac{R_{pl}}{3}, \quad \text{opaque.} \quad (2)$$

Here and below the factor 3 is a putative choice, made in view of other studies of kinetic plasma dynamics. The e^+e^- pair and photon chemical equilibration condition is approximately the same as the opaqueness condition,

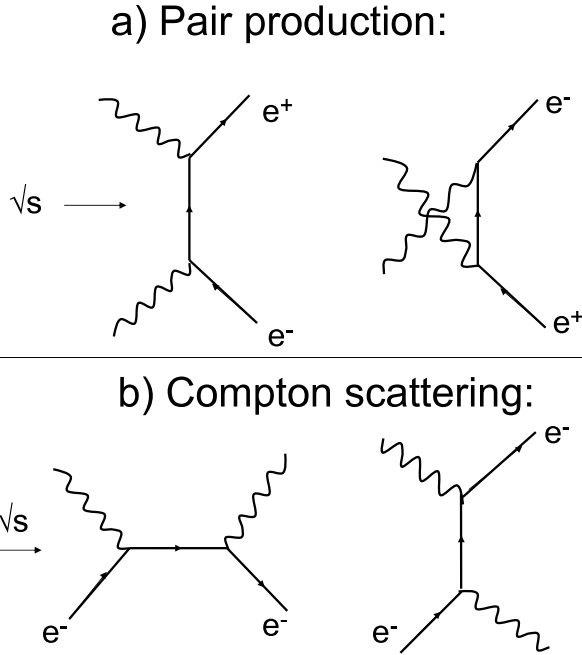


FIG. 1: Feynman diagrams for (a) the creation of the electron-positron pair on top and (b) Compton scattering on the bottom, where incoming particles are on the left side.

Eq.(2) for photons participating in the pair production reaction Eq.(4):

$$L_{\gamma\gamma\rightarrow ee} \leq \frac{R_{pl}}{3}, \quad \text{chemical equilibrium.} \quad (3)$$

The free-streaming and opaqueness conditions are up to numerical evaluation the same.

We consider the mean free path L_γ and γ equilibration by Dirac pair production/annihilation reaction:

$$\gamma + \gamma \leftrightarrow e^+ + e^-, \quad (4)$$

and by Compton scattering:

$$\gamma + e^\pm \leftrightarrow \gamma + e^\pm, \quad (5)$$

for which the Feynman diagrams are shown in Fig. 1.

However, the evaluation of chemical equilibration of electrons and positrons is in essence different, these particles will continue to rescatter even after all photons have left, and e^-, e^+ can pair annihilate into photons. We obtain the mean free path L_{e^-, e^+} and the e^+e^- pair equilibration considering Møller:

$$e^\pm e^\pm \leftrightarrow e^\pm e^\pm, \quad (6)$$

and Bhabha scattering:

$$e^+e^- \leftrightarrow e^+e^-, \quad (7)$$

for which the Feynman diagrams are shown in Fig. 2.

We evaluate using a Lorentz covariant procedure the invariant reaction rates using methods developed first

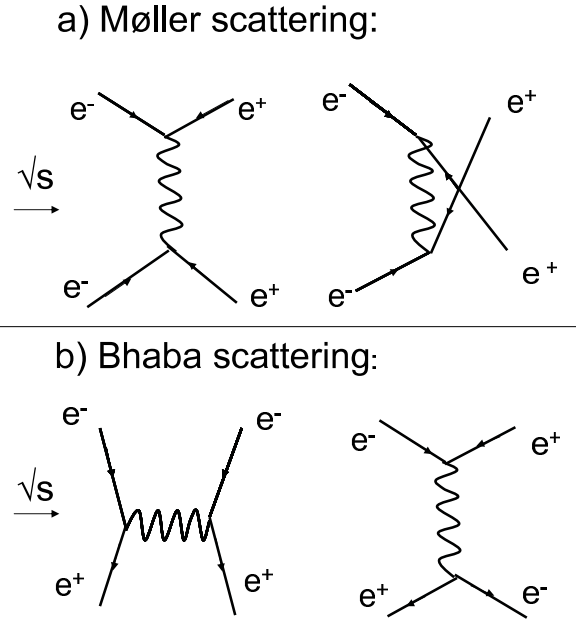


FIG. 2: Feynman diagrams for (a) Møller scattering on top and (b) Bhabha scattering on bottom, where incoming particles are on the left side.

for strange quark pair production in the quark gluon plasma [5, 6]. We extend these methods to scattering reactions which do not change the number of particles.

Our kinetic equations describing the rates and particle multiplicity evolution are obtained from the Boltzmann equation, integrated over the momentum part of the phase space, assuming thermal distribution. As a result, we obtain thermally averaged reaction relaxation time. This approach is appropriate to identify the domain of T in which reactions are fast enough to maintain thermal and chemical equilibrium. However, a future study will need to address how the thermal distribution is established. We also see a need to consider in a more complete transport approach the motion of particles found in high energy tail of distribution, which will be first to escape the plasma drop. However, these particles contribute little to the bulk properties.

We observe that the rates for reactions considered here had been obtained by the other methods, using cross sections [7] and applied for astrophysical environments [8]. Our results differ from those presented in [8], which found that under certain conditions plasma equilibration occurs primarily by pair production, and the Compton scattering has small effect. We show that the Compton scattering is always the dominant process near equilibrium. The work to reconcile [8] with our covariant results continues. One possible source of discrepancy is that in [7] the Lorentz-invariant form of distribution function [see Eq.(8)] is not used in the rate evaluation procedure which involves a later change of reference frames. Therefore our Lorentz covariant results are different and amend this earlier work.

We do not consider the three-body reactions. Their rates are proportional to an additional factor α/π , and thus in general are slower than two-body reactions considered here. We find that Bhabha and Møller processes are much faster than other reactions considered. However, if Bremsstrahlung is about $\alpha = 1/137$ times slower than Bhabha and Møller scatterings, it could still be faster, or of the same order of magnitude, as Compton and pair production. Bremsstrahlung and the related backward processes could therefore somewhat shorten photon equilibration, perhaps visible in some domain of T . We leave this to future study.

Our paper is organized as follows: In section II we review the physical properties (subsection II A) of EP³ plasma, and present (subsection II B) the master equations for chemical equilibration of the plasma components under the assumption that particles are in thermal equilibrium. We introduce $\tau_{\gamma\gamma}^{ch}$, the relaxation time for photon chemical equilibration, in terms of thermal reaction rates, and relate $c\tau_{\gamma\gamma}^{ch}$ to the mean free path for pair production.

In Sec. III we obtain the analytical expressions for the thermal mean free paths for scattering in EP³ plasma. In Sec. III A we review equations for mean free paths and Lorentz-invariant rate calculations. In Sec. III B we review cross sections for pair production and annihilation and Compton scattering as functions of the energy of interacting particles. In Sec. III C we obtain the Lorentz-invariant rate for pair production and annihilation. Similar invariant rate calculations were done before for the strange quark pair production in Refs. [5] and [6]. We perform the required integration by a method similar to [6], and muon pair production [1] we considered earlier. In the following sections we extend that method to Compton (Sec. III D), Møller and Bhabha (Sec. III E) invariant rates. To remove the Coulomb divergence in integrals we introduce a thermal screening photon (Debye) mass, induced by plasma oscillations.

Sec. IV contains our numerical results. In Sec. IV A we look in depth at photon-electron interactions and the Thompson limit. In Sec. IV B we evaluate the photon and electron scattering lengths, and discuss maximum possible plasma size at a given energy. This evaluation is carried out taking account of all quantum physics Fermi and Bose statistic effects in order to be applicable in the high density domain, and we apply the Lorentz-invariant rates method which include medium quantum effects. We connect our results to the Boltzmann limit in Sec. IV C.

In Sec. V we discuss the physical consequences, applications, and present our conclusions.

II. STATISTICAL PROPERTIES OF EP³ PLASMA

A. Relativistic Gas

Up to QED interaction $\mathcal{O}(\alpha)$ effects we can describe the particle content in a plasma using, respectively, rel-

ativistic covariant Fermi and Bose momentum distributions:

$$f_{e^\pm} = \frac{1}{\Upsilon_e^{-1} e^{(u \cdot p_e \pm \nu_e)/T} + 1}, \quad f_\gamma = \frac{1}{\Upsilon_\gamma^{-1} e^{u \cdot p_\gamma/T} - 1}, \quad (8)$$

Υ_i ($i = e, \gamma$) is the fugacity of a given particle. When $\Upsilon_i = 1$, the particle yield is in chemical equilibrium. For $\Upsilon_i = 1$ this distribution maximizes the entropy content at a fixed particle energy [9].

The Lorentz-invariant exponents involve the scalar product of the particle 4-momentum p_i^μ with the local 4-vector of velocity u^μ . In the absence of matter flow we have in the rest frame of the thermal bath (laboratory frame)

$$u^\mu = (1, \vec{0}), \quad p_i^\mu = (E_i, \vec{p}_i). \quad (9)$$

When the electron chemical potential ν_e is small, $\nu_e \ll T$, the number of particles and antiparticles is the same, $n_{e^-} = n_{e^+}$. Physically, it means that the number of e^+e^- pairs produced dominates the residual matter electron yield. Here we will set $\nu_e = 0$, and will consider elsewhere the case for very low density plasma where chemical potential may become important.

The particle density and plasma energy density can be evaluated using relativistic expressions:

$$n_i = \int g_i f_i(p) d^3p; \quad E = \int \sum_i g_i E_i f_i(p) d^3p V, \quad (10)$$

where $E_i = \sqrt{m_i^2 + \vec{p}^2}$, $f_i(p)$ is the momentum distribution of the particle $i \in \gamma, e^\pm$, and g_i is its degeneracy; $g_i = 2$ for photons, electrons and positrons. In Fig. 3 we present electron-positron and photon densities as functions of temperature. At our range of temperatures their values are much larger than atomic density, 10^{23} cm^{-3} .

After integration we obtain

$$\frac{\mathcal{E}}{V} = \epsilon = \frac{\pi^2}{30} g(T) T^4. \quad (11)$$

At a temperature $T \ll m_e$ we only have truly massless photons and $g(T) = 2\gamma$. Once the temperature approaches and increases beyond m_e , we find $g \simeq g'(T) \simeq 2\gamma + (7/8)(2_{e^-} + 2_{e^+}) = 5.5$.

In a classical case, $\Upsilon \ll 1$, there is no difference between Bose and Fermi particles. We have for massless particles ($m/T \rightarrow 0$)

$$E = 3NT, \quad N = \Upsilon \frac{g}{\pi^2} T^3 V, \quad (12)$$

where $g = 6$.

B. Approach to equilibrium

In our approach new photons are produced by a pair annihilation reaction, Eq (4). If we assume that thermal

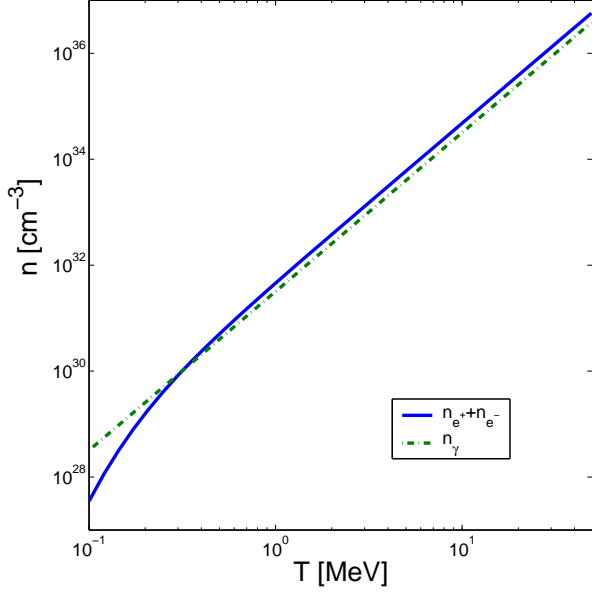


FIG. 3: Electron-positron (blue solid line) and photon (green dash-dotted line) densities as functions of temperature.

equilibrium is established faster than chemical, then the photon density evolution equations and chemical equilibrium conditions are similar to those for muon production, studied in [1]:

$$\frac{1}{V} \frac{dN_\gamma}{dt} = (\Upsilon_e^2 - \Upsilon_\gamma^2) R_{\gamma\gamma \leftrightarrow e^+e^-}, \quad (13)$$

where

$$R_{\gamma\gamma \leftrightarrow e^+e^-} = \frac{1}{\Upsilon_\gamma^2} \frac{dW_{\gamma\gamma \rightarrow e^+e^-}}{dV dt} = \frac{1}{\Upsilon_e^2} \frac{dW_{e^+e^- \rightarrow \gamma\gamma}}{dV dt}, \quad (14)$$

$dW_{\gamma\gamma \rightarrow e^+e^-}/dV dt$ and $dW_{e^+e^- \rightarrow \gamma\gamma}/dV dt$ are Lorentz-invariant rates for pair production and annihilation reactions, respectively. Rate $R_{\gamma\gamma \leftrightarrow e^+e^-}$ does not depend on Υ_i in limit of a classical Boltzmann distribution. The EP³ plasma is in *relative chemical equilibrium* for $\Upsilon_\gamma < 1$ when

$$\Upsilon_e = \Upsilon_\gamma. \quad (15)$$

In relative equilibrium at a given instant the considered reaction, for example (4), is in equilibrium. However for other reactions this condition may not be an equilibrium (for example for reaction $ee \leftrightarrow ee\gamma$) and then the system can move to another relative equilibrium condition with time. The relative chemical equilibrium occurs when crossing different time scale governs relevant “chemical” reactions. At $\Upsilon_{e,\gamma} \rightarrow 1$ (and for all others particles in the system, if any, $\Upsilon_i \rightarrow 1$) all reactions are in equilibrium and the system achieves full chemical equilibrium.

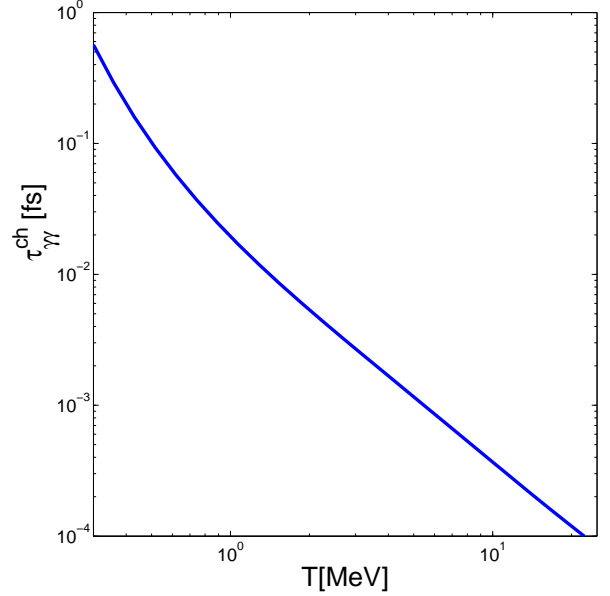


FIG. 4: The relaxation time for pair and photon chemical equilibration.

We introduce pair production relaxation time defined by:

$$\tau_{\gamma\gamma}^{ch} = \frac{1}{2\Upsilon_e} \frac{dn_\gamma/d\Upsilon_\gamma}{R_{\gamma\gamma \leftrightarrow e^+e^-}}, \quad (16)$$

then for the simplest case $T(t) = \text{Const.}$ and $R(t) = \text{Const.}$ the equation for Υ_γ is

$$\frac{d\Upsilon_\gamma}{dt} = (\Upsilon_e^2 - \Upsilon_\gamma^2) \frac{1}{2\Upsilon_e \tau_{\gamma\gamma}^{ch}}. \quad (17)$$

The relaxation time vs temperature for photon and e^+e^- pair chemical equilibration is shown in figure 4. The rates and relaxation times are discussed in depth in [1].

To understand better the choice of definition of relaxation time $\tau_{\gamma\gamma}^{ch}$, Eq.(16), we assume $\Upsilon_e = \text{const.}$ and introduce variable $\gamma = \Upsilon_\gamma/\Upsilon_e$, which shows deviation from chemical equilibrium. Then the equation for γ is

$$\frac{d\gamma}{dt} = (1 - \gamma^2) \frac{1}{2\tau_{\gamma\gamma}^{ch}}. \quad (18)$$

The relaxation time is defined as the time for particle multiplicity to reach the magnitude of equilibrium value. Note that the relaxation time for a particle (in this example photon) production in a two-to-two-particles reaction, Eq.(16), changes by a factor Υ_i^{-1} , where i denotes the initial particle in a reaction (here e^\pm). The physical reason why the relaxation time is proportional to Υ_i^{-1} is that the collision rate drops by this factor, due to reduced density of plasma.

In the simple case considered here, e^+e^- pair production and annihilation are chemically equilibrated when condition Eq.(3) is satisfied.

III. MEAN FREE PATHS OF PHOTON AND ELECTRON (POSITRON) IN $e^+e^- \gamma$ PLASMA

A. Reaction rate and mean free paths

In order to be in thermal and chemical equilibrium plasma must be opaque for the reactions, which establish this equilibrium. The major reactions which may establish thermal and/or chemical equilibrium between photons and e^+e^- pairs are Compton scattering and pair production and annihilation. e^+e^- can also participate in Møller scattering Eq.(6) and Bhabha scattering Eq.(7). Here we consider the reaction

$$1 + 2 \leftrightarrow 3 + 4, \quad (19)$$

For reaction Eq.(19), the thermally averaged cross section is

$$\langle v\sigma_{12 \rightarrow 34} \rangle = \frac{\Upsilon_1 \Upsilon_2 R_{12 \leftrightarrow 34}}{n_1 n_2}, \quad (20)$$

(velocity $v = c$ for photons scattering, we take $c = 1$) and the mean free path is

$$L_{1(2)} = \frac{1}{n_{2(1)} \langle v\sigma_{12 \rightarrow 34} \rangle} = \frac{n_{1(2)}}{\Upsilon_1 \Upsilon_2 R_{12 \leftrightarrow 34}}, \quad (21)$$

where v is the relative velocity of interacting particles and $\sigma_{12 \rightarrow 34}$ is cross section.

Rate R is connected to Lorentz-invariant reaction rates by Eq.(14). The equation for rate R is [5, 6]

$$R_{12 \leftrightarrow 34} = \frac{1}{1 + I} \frac{g_\gamma^2}{(2\pi)^8} \int \frac{d^3 p_1}{2E_1} \int \frac{d^3 p_2}{2E_2} \int \frac{d^3 p_3}{2E_3} \int \frac{d^3 p_4}{2E_4} \times \\ \times \delta^4(p_1 + p_2 - p_3 - p_4) \sum_{\text{spin}} |\langle p_1 p_2 | M_{12 \rightarrow 34} | p_3 p_4 \rangle|^2 \times \\ f_1(p_1) f_2(p_2) f_3(p_3) f_4(p_4) (\Upsilon_1 \Upsilon_2 \Upsilon_3 \Upsilon_4)^{-1} e^{\frac{u \cdot (p_1 + p_2)}{T}}, \quad (22)$$

where $I = 1$, if there are identical particles in the initial or final state.

Rate $R_{12 \leftrightarrow 34}$ is the same for reactions in both directions, because of time reversal symmetry of the matrix element:

$$|\langle p_1 p_2 | M_{12 \rightarrow 34} | p_3 p_4 \rangle|^2 = |\langle p_3 p_4 | M_{34 \rightarrow 12} | p_1 p_2 \rangle|^2. \quad (23)$$

In the evaluation of matrix element we will use Mandelstam variables: s , u , and t . For reaction (19) we have

$$s = (p_1 + p_2)^2; \quad u = (p_3 - p_2)^2; \quad t = (p_3 - p_1)^2; \quad (24)$$

and $s + u + t = m_1^2 + m_2^2 + m_3^2 + m_4^2$.

If we exchange particles 2 and 3 as $1 + 3 \leftrightarrow 2 + 4$ or $p_2 \leftrightarrow p_3$, the matrix element for this reaction can be obtained from the matrix element for reaction Eq.(19) by crossing s and t :

$$|M_{12 \rightarrow 34}(s, t, u)|^2 = \pm |M_{13 \rightarrow 24}(t, s, u)|^2. \quad (25)$$

The sign before the matrix element may change to opposite depending if one of the particles, 3 or 2, changes from particle to antiparticle after crossing.

For example, for pair production and annihilation and Compton scattering particles 1,2 are photons and particles 3,4 are electron and positron. The matrix elements for these reactions is defined by Feynman diagrams in Figs. 1(a) and (b), respectively. The matrix element averaged over final states spins for pair production and annihilation is [12], [13]

$$|M_{\gamma\gamma \leftrightarrow ee}|^2 = 32\pi^2 \alpha^2 \left(-4 \left(\frac{m^2}{m^2 - t} + \frac{m^2}{m^2 - u} \right)^2 + \frac{4m^2}{m^2 - t} + \frac{4m^2}{m^2 - u} + \frac{m^2 - u}{m^2 - t} + \frac{m^2 - t}{m^2 - u} \right), \quad (26)$$

The matrix element for Compton scattering is

$$|M_{\gamma e \leftrightarrow \gamma e}|^2 = 32\pi^2 \alpha^2 \left(4 \left(\frac{m^2}{m^2 - s} + \frac{m^2}{m^2 - u} \right)^2 - \frac{4m^2}{m^2 - s} - \frac{4m^2}{m^2 - u} - \frac{m^2 - u}{m^2 - s} - \frac{m^2 - s}{m^2 - u} \right), \quad (27)$$

The matrix elements for these reactions are connected by Eq.(25).

Similarly, crossing s and u allows us to find

$$|M_{12 \rightarrow 34}(s, t, u)|^2 = \pm |M_{23 \rightarrow 14}(u, t, s)|^2. \quad (28)$$

The matrix elements for Møller and Bhabha scattering (diagrams are in Figs. 2 (a) and (b), respectively) are connected by Eq.(28). The Møller scattering matrix element is (similar to [14])

$$|M_{e^\pm e^\pm}|^2 = 2^6 \pi^2 \alpha^2 \left\{ \frac{s^2 + u^2 + 8m^2(t - m^2)}{2(t - m_\gamma^2)^2} + \frac{s^2 + t^2 + 8m^2(u - m^2)}{2(u - m_\gamma^2)^2} + \frac{(s - 2m^2)(s - 6m^2)}{(t - m_\gamma^2)(u - m_\gamma^2)} \right\}, \quad (29)$$

To obtain the Bhabha scattering matrix element we need to cross u and s , Eq.(28) in Møller scattering matrix element (29). We obtain

$$|M_{e^+ e^-}|^2 = 2^6 \pi^2 \alpha^2 \left\{ \frac{s^2 + u^2 + 8m^2(t - m^2)}{2(t - m_\gamma^2)^2} + \frac{u^2 + t^2 + 8m^2(s - m^2)}{2(s - m_\gamma^2)^2} + \frac{(u - 2m^2)(u - 6m^2)}{(t - m_\gamma^2)(s - m_\gamma^2)} \right\}, \quad (30)$$

and the photon thermal (Debye) mass m_γ will be defined in Sec. III E.

B. Pair annihilation and production and Compton scattering cross sections

In this section we consider cross sections for pair annihilation and production and Compton scattering as functions of energy. The cross section $\sigma(s)$ can be obtained by averaging the matrix element over the t variable. Similar calculations were done in [10] for heavy quarks production in quark gluon plasma. In the case of Compton scattering we obtain

$$\begin{aligned} \sigma_{\gamma e \leftrightarrow \gamma e}(s) &= \frac{1}{16\pi(s - m^2)^2} \int_{-(s - m^2)^2/s}^0 dt |M_{\gamma e^\pm}|^2 \\ &= \frac{2\pi\alpha^2}{(s - m^2)^2} \left(\frac{2(s - m^2)^2 s - (s - m^2)^3}{2s^2} + 8m^2 - \left(\frac{8m^4}{s - m^2} + 4m^2 - (s - m^2) \right) \ln \frac{s}{m^2} \right) \end{aligned} \quad (31)$$

For pair production and annihilation we have (similar results as in [11])

$$\begin{aligned} \sigma_{\gamma\gamma \rightarrow ee}(s) &= \frac{1}{16\pi s^2} \int_{m^2 - s(1 + \sqrt{1 - 4m^2/s})/2}^{m^2 - s(1 - \sqrt{1 - 4m^2/s})/2} dt |M_{\gamma\gamma \leftrightarrow ee}|^2 \\ &= \frac{4\pi\alpha^2}{s^3} \left((s^2 + 4m^2 s - 8m^4) \ln \frac{\sqrt{s} + \sqrt{s - 4m^2}}{\sqrt{s} - \sqrt{s - 4m^2}} - (s + 4m^2) \sqrt{s(s - 4m^2)} \right). \end{aligned} \quad (32)$$

$$\begin{aligned} \sigma_{ee \rightarrow \gamma\gamma}(s) &= \frac{1}{32\pi s(s - m^2)} \int_{m^2 - s(1 + \sqrt{1 - 4m^2/s})/2}^{m^2 - s(1 - \sqrt{1 - 4m^2/s})/2} dt |M_{\gamma\gamma \leftrightarrow ee}|^2 \\ &= \frac{2\pi\alpha^2}{s^2(s - m^2)} \left((s^2 + 4m^2 s - 8m^4) \ln \frac{\sqrt{s} + \sqrt{s - 4m^2}}{\sqrt{s} - \sqrt{s - 4m^2}} - (s + 4m^2) \sqrt{s(s - 4m^2)} \right). \end{aligned} \quad (33)$$

Note that there is an extra $1/2$ factor in the equation for pair annihilation because we have two identical particles; that is a symmetrical wave function in the final state. Similarly, in the reaction rate R we add an additional factor $1/2$ when there are initial identical particles. In the backward reaction there is also a factor $1/2$ from the definition of cross section. Therefore the rate is symmetrical in both reaction directions: pair formation and annihilation.

In Fig. 5 we show cross sections (31)-(32) as functions of total energy of particles in reaction $s^{1/2}$ (center of mass frame) for pair production (solid blue line), annihilation (dash-dotted green line) and for Compton scattering (dashed red line).

At high energy $E_{\text{tot}} \gg m$ the cross section dependence on energy is a power law,

$$\sigma = A \left(\frac{E_{\text{tot}}}{1 \text{ MeV}} \right)^N. \quad (34)$$

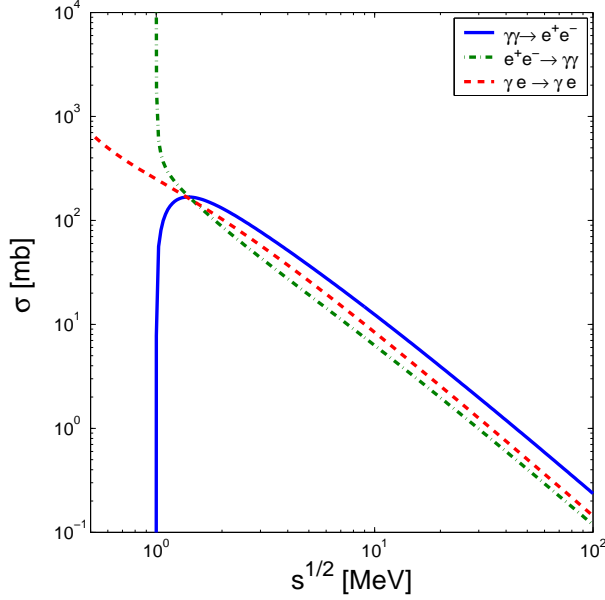


FIG. 5: The cross sections for pair production (solid blue line) and annihilation (dash-dotted green line) in the center of mass frame, and for Compton scattering (dashed red line) in the electron rest frame are shown as functions of total energy of interacting particles E_{tot} .

TABLE I: Values of N and A for power law energy dependence of cross section high energy tail, Eq.(34), for cross sections presented in Fig. 5

Reaction	N	A (mb)
$\gamma e \leftrightarrow \gamma e$	-1.7	330
$\gamma\gamma \leftrightarrow e^+e^-$	-1.7	410
$e^+e^- \leftrightarrow \gamma\gamma$	-1.7	309

The coefficients A and N are shown in Table I.

The decrease of cross sections with particles energy increase could result in the early escape (freeze-out) of very high energy particles from the plasma which would impact heavier particle (muon, meson) production. However, this has no material impact on our present considerations.

C. Lorentz-invariant pair production and annihilation rates

The equation for pair production and annihilation rate $R_{\gamma\gamma \leftrightarrow ee}$ ($R_{12 \leftrightarrow 34}$) in Eq.(21) is similar to the equation for the rate of muon production in photons fusion that we presented in [1]:

$$\begin{aligned}
R_{\gamma\gamma \leftrightarrow ee} &= \frac{g_\gamma^2}{2(2\pi)^8} \int \frac{d^3 p_1^\gamma}{2E_1^\gamma} \int \frac{d^3 p_2^\gamma}{2E_2^\gamma} \int \frac{d^3 p_3^e}{2E_3^e} \int \frac{d^3 p_4^e}{2E_4^e} \times \\
&\times \delta^4(p_1^\gamma + p_2^\gamma - p_3^e - p_4^e) \sum_{\text{spin}} | \langle p_1^\gamma p_2^\gamma | M_{\gamma\gamma \rightarrow ee} | p_3^e p_4^e \rangle |^2 \\
&\times f_\gamma(p_1^\gamma) f_\gamma(p_2^\gamma) f_e(p_3^e) f_e(p_4^e) \Upsilon_\gamma^{-2} \Upsilon_e^{-2} e^{u \cdot (p_1^\gamma + p_2^\gamma)/T}, \quad (35)
\end{aligned}$$

We define

$$\begin{aligned}
\mathbf{q} &= p_1 + p_2; & \mathbf{p} &= \frac{1}{2}(p_1 - p_2); \\
\mathbf{q}' &= p_4 + p_3; & \mathbf{p}' &= \frac{1}{2}(p_4 - p_3);
\end{aligned} \quad (36)$$

and then we have $\mathbf{q}^2 = q_0^2 - q^2 = q_0'^2 - q'^2 = s \geq 2m^2$ and

$$\begin{aligned}
p_1 &= \frac{\mathbf{q}}{2} + \mathbf{p}; & p_2 &= -\mathbf{p} + \frac{1}{2}\mathbf{q}; \\
p_3 &= \frac{\mathbf{q}}{2} - \mathbf{p}'; & p_4 &= \frac{\mathbf{q}}{2} + \mathbf{p}'.
\end{aligned} \quad (37)$$

Using

$$\int \frac{d^3 p}{2E} = \int d^4 p \delta(p^2 - m^2) \theta(p_0) \equiv \int d^4 p \delta_0(p^2 - m^2), \quad (38)$$

and $p_{3,4}^2 - m^2 = 0$ and $p_{1,2}^2 = 0$, we obtain:

$$\begin{aligned}
R_{\gamma\gamma \leftrightarrow ee} &= \frac{g_\gamma^2}{2(2\pi)^8} \int d^4 q \int d^4 p \int d^4 p' \delta_0(p_1^2) \delta_0(p_2^2) \\
&\times \delta_0(p_3^2 - m^2) \delta_0(p_4^2 - m^2) \Upsilon_\gamma^{-2} \Upsilon_e^{-2} \exp(q_0/T) \\
&\times \sum |M_{\gamma\gamma \rightarrow ee}|^2 f_\gamma(p_1^0) f_e(p_3^0) f_\gamma(p_2^0) f_e(p_4^0). \quad (39)
\end{aligned}$$

The integrals from Eq.(39) can be evaluated in spherical coordinates. The angle coordinates are chosen with respect to the direction of $\vec{q} = \vec{p}_3 + \vec{p}_1$:

$$q_\mu = (q_0, 0, 0, q), \quad p_\mu = (p_0, p \sin \theta, 0, p \cos \theta),$$

$$p'_\mu = (p'_0, p' \sin \phi \sin \chi, p' \sin \phi \cos \chi, p' \cos \phi).$$

Using Eqs. (37) and delta functions we obtain the equations:

$$p_0^2 - p^2 + \frac{s}{4} + p_0 q_0 - p q \cos(\theta) - m^2 = 0; \quad (40)$$

$$p_0'^2 - p'^2 + \frac{s}{4} - p_0' q_0 + p' q \cos(\theta) - m^2 = 0; \quad (41)$$

$$p_0'^2 - p'^2 + \frac{s}{4} + p_0' q_0 - p' q \cos(\phi) = 0; \quad (42)$$

$$p_0'^2 - p'^2 + \frac{s}{4} - p_0' q_0 + p' q \cos(\phi) = 0; \quad (43)$$

then using $\delta(f(x)) = \sum_i 1/|f'(x_i)| \delta(x - x_i)$, we can rewrite the integral (similar to [6]) as

$$\begin{aligned}
R_{\gamma\gamma\leftrightarrow ee} &= \frac{g_\gamma^2}{(2\pi)^6 16} \int_{2m}^\infty dq_0 \int_0^{\sqrt{q_0^2 - s}} dq \int_{q_1}^{q_2} dp_0 \int_{q_1^*}^{q_2^*} dp_0' \int_0^\infty dp \int_0^\infty dp' \int_{-1}^1 d(\cos\theta) \int_{-1}^1 d(\cos\phi) \int_0^{2\pi} d\chi \sum |M_{\gamma\gamma\rightarrow ee}|^2 \\
&\times \delta\left(p - \left(p_0^2 + \frac{s}{4} - m^2\right)^{1/2}\right) \delta\left(p' - \left(p_0'^2 + \frac{s}{4}\right)^{1/2}\right) \delta\left(\cos\phi - \frac{q_0 p_0'}{q p'}\right) \delta\left(\cos\theta - \frac{q_0 p_0}{p q}\right) \\
&\times f_\gamma\left(\frac{q_0}{2} + p_0'\right) f_\gamma\left(\frac{q_0}{2} - p_0'\right) \Upsilon_e^{-2} \Upsilon_\gamma^{-2} f_e\left(\frac{q_0}{2} + p_0\right) f_e\left(\frac{q_0}{2} - p_0\right) \exp(q_0/T), \tag{44}
\end{aligned}$$

where

$$q_{1,2} = \pm \frac{q}{2} \sqrt{1 - \frac{4m^2}{s}}; \tag{45}$$

$$q_{1,2}^* = \pm \frac{q}{2}. \tag{46}$$

$q_{1,2}$ and $q_{1,2}^*$ come from constrains $\cos\theta, \cos\phi < 1$ and δ functions in Eq.(44).

The integration over $p, p', \cos\theta$, and $\cos\phi$ can be done analytically considering δ functions. Other integrals can be evaluated numerically. In order to simplify numerical integration we introduce dimensionless variables:

$$q = (q_0^2 - 4m^2)^{1/2} z; \tag{47}$$

$$p_0 = \frac{q}{2} \sqrt{1 - \frac{4m^2}{s}} x; \tag{48}$$

$$p_0' = \frac{q}{2} y; \tag{49}$$

$0 < z < 1; -1 < x(y) < 1$.

In these variables, using the δ function in Eq.(44), we obtain for u and t :

$$\begin{aligned}
u &= (p - p')^2 = m^2 - \frac{s}{2} + \frac{s}{2} \sqrt{1 - \frac{4m^2}{s}} \times \\
&(xy - \sqrt{(1-x^2)(1-y^2)} \sin\chi);
\end{aligned}$$

$$\begin{aligned}
t &= (p + p')^2 = m^2 - \frac{s}{2} - \frac{s}{2} \sqrt{1 - \frac{4m^2}{s}} \times \\
&(xy - \sqrt{(1-x^2)(1-y^2)} \sin\chi). \tag{50}
\end{aligned}$$

Using new variables (47)-(49) the Eq. (35) is

$$\begin{aligned}
R_{\gamma\gamma\rightarrow ee} &= \frac{g_\gamma^2}{2^{12} \pi^6} \int_{2m}^\infty dq_0 \exp(q_0) \int_0^1 dz z^2 (q_0^2 - 4m^2)^{3/2} \\
&\times \int_0^{2\pi} d\chi \int_{-1}^1 dx \int_{-1}^1 dy \sqrt{1 - \frac{4m^2}{s}} \sum |M_{\gamma\gamma\rightarrow ee}|^2 \\
&\times \Upsilon_e^{-2} f_\gamma\left(\frac{q_0}{2} + p_0'\right) f_\gamma\left(\frac{q_0}{2} - p_0'\right) \\
&\times \Upsilon_\gamma^{-2} f_e\left(\frac{q_0}{2} + p_0\right) f_e\left(\frac{q_0}{2} - p_0\right). \tag{51}
\end{aligned}$$

The matrix element is defined by Eq. 26.

D. Compton scattering Lorentz-invariant rate

The equation for the Compton scattering rate is

$$\begin{aligned}
R_{\gamma e} &= \frac{g_e g_\gamma}{(2\pi)^8} \int \frac{d^3 p_3^e}{2E_3^e} \int \frac{d^3 p_1^\gamma}{2E_1^\gamma} \int \frac{d^3 p_3^e}{2E_4^e} \int \frac{d^3 p_2^\gamma}{2E_2^\gamma} \tag{52} \\
&\times \delta^4(p_1^\gamma + p_3^e - p_4^e - p_2^\gamma) \sum_{\text{spin}} |\langle p_1^\gamma p_3^e | M_{\gamma e \rightarrow \gamma e} | p_2^\gamma p_4^e \rangle|^2 \\
&\times f_\gamma(p_{1\gamma}) f_\gamma(p_{2\gamma}) f_e(p_3^e) f_e(p_4^e) \Upsilon_\gamma^{-2} \Upsilon_e^{-2} e^{u \cdot (p_3^e + p_1^\gamma)/T}
\end{aligned}$$

The Feynman diagrams for Compton scattering are shown in figure 1 (b). The matrix element for Compton scattering, Eq.(27), can be obtained by crossing t and s , Eq.(25), in the matrix element for pair production and annihilation, Eq.(26).

In this case $s = (\mathbf{p}_3 + \mathbf{p}_1)^2$, $t = (\mathbf{p}_1 - \mathbf{p}_2)^2$ and $u = (\mathbf{p}_3 - \mathbf{p}_2)^2$.

We need to cross p_2 and p_3 in variables q, p and p' definition, Eq.(36).

In this case we have $\mathbf{q}^2 = q_0^2 - q^2 = q_0'^2 - q'^2 = s \geq m^2$ and

$$\begin{aligned}
p_1 &= \frac{\mathbf{q}}{2} + \mathbf{p}; & p_2 &= -\mathbf{p}' + \frac{1}{2}\mathbf{q}; \\
p_3 &= \frac{\mathbf{q}}{2} - \mathbf{p}; & p_4 &= \frac{\mathbf{q}}{2} + \mathbf{p}'. \tag{53}
\end{aligned}$$

Then, similar to pair production and annihilation rate, we obtain:

$$\begin{aligned}
R_{e\gamma} &= \frac{g_e g_\gamma}{(2\pi)^8} \int d^4 q \int d^4 p \int d^4 p' \delta(p_1^2) \delta(p_3^2 - m^2) \delta(p_4^2 - m^2) \delta(p_2^2) \theta(p_1^0) \theta(p_2^0) \theta(p_3^0) \theta(p_4^0) \\
&\times \sum |M_{\gamma e \rightarrow \gamma e}|^2 \Upsilon_e^{-2} f_e(p_3^0) f_\gamma(p_1^0) \Upsilon_\gamma^{-2} f_\gamma(p_2^0) f_e(p_4^0) \exp(q_0/T). \tag{54}
\end{aligned}$$

Using Eqs. (53) and δ functions from Eq.(54) we obtain the equations:

$$p_0^2 - p^2 + \frac{s}{4} + p_0 q_0 - pq \cos(\theta) = 0; \tag{55}$$

$$p_0^2 - p^2 + \frac{s}{4} - p_0 q_0 + pq \cos(\theta) - m^2 = 0; \tag{56}$$

$$p_0'^2 - p'^2 + \frac{s}{4} + p_0' q_0 - p' q \cos(\phi) - m^2 = 0; \tag{57}$$

$$p_0'^2 - p'^2 + \frac{s}{4} - p_0' q_0 + p' q \cos(\phi) = 0; \tag{58}$$

then using $\delta(f(x)) = \sum_i 1/|f'(x_i)|\delta(x - x_i)$, we can rewrite the integral as

$$\begin{aligned}
R_{e\gamma} &= \frac{2g_e g_\gamma}{(2\pi)^6 16} \int_m^\infty dq_0 \int_0^{\sqrt{q_0^2 - s}} dq \int_{q_1}^{q_2} dp_0 \int_{q_1^*}^{q_2^*} dp_0' \int_0^\infty dp \int_0^\infty dp' \int_{-1}^1 d(\cos \theta) \int_{-1}^1 d(\cos \phi) \int_0^{2\pi} d\chi \\
&\times \sum |M_{e\gamma \rightarrow e\gamma}|^2 \delta\left(p - \left(p_0^2 + \frac{s}{4} - \frac{m^2}{2}\right)^{1/2}\right) \delta\left(p' - \left(p_0'^2 - \frac{m^2}{2} + \frac{s}{4}\right)^{1/2}\right) \delta\left(\cos \phi - \frac{q_0 p_0'}{qp'} + \frac{m^2}{2qp'}\right) \\
&\times \delta\left(\cos \theta - \frac{q_0 p_0}{pq} - \frac{m^2}{2qp}\right) f_e\left(\frac{q_0}{2} - p_0\right) f_\gamma\left(\frac{q_0}{2} + p_0\right) \Upsilon_e^{-2} \Upsilon_\gamma^{-2} f_\gamma\left(\frac{q_0}{2} - p_0'\right) f_e\left(\frac{q_0}{2} + p_0'\right) \exp(q_0/T), \tag{59}
\end{aligned}$$

where in this case

$$q_{1,2} = -\frac{m^2 q_0}{2s} \pm \frac{q}{2} \left(1 - \frac{m^2}{s}\right); \tag{60}$$

$$q_{1,2}^* = \frac{m^2 q_0}{2s} \pm \frac{q}{2} \left(1 - \frac{m^2}{s}\right). \tag{61}$$

The integration over p , p' , $\cos \theta$ and $\cos \phi$ can be done analytically considering δ functions. Other integrals can be evaluated numerically. In order to simplify numerical integration we introduce dimensionless variables:

$$q = (q_0^2 - m^2)^{1/2} z; \tag{62}$$

$$p_0 = -\frac{m^2 q_0}{2s} + \frac{q}{2} \left(1 - \frac{m^2}{s}\right) x, \tag{63}$$

$$p_0' = \frac{m^2 q_0}{2s} + \frac{q}{2} \left(1 - \frac{m^2}{s}\right) y, \tag{64}$$

$$0 < z < 1; -1 < x(y) < 1.$$

With these variables, using the δ function in Eq.(59), we obtain for u and t :

$$\begin{aligned}
u &= (p - p')^2 = m^2 - \frac{s}{2} + \frac{m^4}{2s} + \frac{s}{2} \left(1 - \frac{m^2}{s}\right)^2 \\
&\times (xy - \sqrt{(1-x^2)(1-y^2)} \sin \chi);
\end{aligned}$$

$$\begin{aligned}
t &= (p + p')^2 = m^2 - \frac{s}{2} - \frac{m^4}{2s} - \frac{s}{2} \left(1 - \frac{m^2}{s}\right)^2 \\
&\times (xy - \sqrt{(1-x^2)(1-y^2)} \sin \chi). \tag{65}
\end{aligned}$$

Then limits for t are $0 > t > -s + 2m^2 - m^4/s$. In the limit $s \gg m^2$ the variables u and t for Compton scattering go to the same limit as u and t for pair production and annihilation, Eq.(50).

Using new variables (62)-(64) the Eq. (52) is

$$\begin{aligned}
R_{e\gamma} &= \frac{g_\gamma g_e}{2^{11}\pi^6} \int_m^\infty dq_0 \exp(q_0) \int_0^1 dz z^2 (q_0^2 - m^2)^{3/2} \int_0^{2\pi} d\chi \int_{-1}^1 dx \int_{-1}^1 dy \left(1 - \frac{m^2}{s}\right)^2 \sum |M_{\gamma e^\pm \rightarrow \gamma e^\pm}|^2 \\
&\times \Upsilon_e^{-2} f_{e^\pm} \left(\frac{q_0}{2} - p_0\right) f_\gamma \left(\frac{q_0}{2} + p_0\right) \Upsilon_\gamma^{-2} f_\gamma \left(\frac{q_0}{2} - p'_0\right) f_e \left(\frac{q_0}{2} + p'_0\right). \tag{66}
\end{aligned}$$

E. Møller and Bhabha scatterings

In this section we consider Møller and Bhabha scatterings, Eq.(6) and Eq.(7), respectively. To remove Coulomb divergence in reaction rates we introduce thermal photon mass induced by Debye screening [15]:

$$m_\gamma = \omega_{pl}, \tag{67}$$

where ω_{pl} is plasma frequency.

$$m_\gamma^2 = \frac{4e^2}{3\pi^2} \int_0^\infty dp p f_F(p). \tag{68}$$

For highly relativistic plasma $T \gg m_e$

$$m_\gamma = \frac{\sqrt{4\pi\alpha}}{3} T. \tag{69}$$

The corresponding thermal mass of electron for high temperatures is [15]

$$m = \frac{\sqrt{4\pi\alpha}}{2\sqrt{2}} T. \tag{70}$$

In our range of temperatures we assume:

$$m^2 = m_e^2 + \frac{4\pi\alpha}{8} T^2. \tag{71}$$

In this section $m_e = 0.5$ MeV is electron mass without thermal effects.

The Feynman diagrams for Møller (a) and Bhabha scatterings (b) are shown in Fig. 2 and the matrix elements are defined by Eqs.(29) and Eq.(30), respectively. In both cases all initial and final particles are massive and have the same mass. After transformations similar to the ones used for Compton scattering the equation for the Møller (Bhabha) rate is

$$\begin{aligned}
R_{ee} &= \frac{1}{1+I} \frac{2g_e^2}{(2\pi)^6 16} \int_{2m}^\infty dq_0 \int_0^{\sqrt{q_0^2 - s}} dq \int_{q_1}^{q_2} dp_0 \int_{q_1^*}^{q_2^*} dp'_0 \int_0^\infty dp \int_0^\infty dp' \int_{-1}^1 d(\cos\theta) \int_{-1}^1 d(\cos\phi) \int_0^{2\pi} d\chi \\
&\times \sum |M_{ee}|^2 \delta\left(p - \left(p_0^2 + \frac{s}{4} - m^2\right)^{1/2}\right) \delta\left(p' - \left(p_0'^2 - m^2 + \frac{s}{4}\right)^{1/2}\right) \delta\left(\cos\phi - \frac{q_0 p'_0}{qp'}\right) \\
&\times \delta\left(\cos\theta - \frac{q_0 p_0}{pq}\right) f_e\left(\frac{q_0}{2} + p_0\right) f_e\left(\frac{q_0}{2} - p_0\right) \Upsilon_e^{-4} f_e\left(\frac{q_0}{2} + p'_0\right) f_e\left(\frac{q_0}{2} - p'_0\right) \exp(q_0/T), \tag{72}
\end{aligned}$$

$$q_{1,2} = \mp \frac{q}{2} \sqrt{\left(1 - \frac{4m^2}{s}\right)}; \tag{73}$$

$$q_{1,2}^* = \mp \frac{q}{2} \sqrt{\left(1 - \frac{4m^2}{s}\right)}. \tag{74}$$

$q_{1,2}$ and $q_{1,2}^*$ come from constraints $\cos\theta, \cos\phi < 1$. Then we introduce dimensionless variables similar to Eqs.(62)-

(64):

$$q = (q_0^2 - 4m^2)^{1/2} z; \tag{75}$$

$$p_0 = \frac{q}{2} \sqrt{\left(1 - \frac{4m^2}{s}\right)} x, \tag{76}$$

$$p'_0 = \frac{q}{2} \sqrt{\left(1 - \frac{4m^2}{s}\right)} y, \tag{77}$$

$0 < z < 1$; $-1 < x(y) < 1$.

With these variables we obtain for u and t :

$$\begin{aligned}
 u &= (p - p')^2 = 2m^2 - \frac{s}{2} + \frac{s}{2} \left(1 - \frac{4m^2}{s}\right) \\
 &\quad \times (xy - \sqrt{(1-x^2)(1-y^2)} \sin \chi); \\
 t &= (p + p')^2 = 2m^2 - \frac{s}{2} - \frac{s}{2} \left(1 - \frac{4m^2}{s}\right) \\
 &\quad \times (xy - \sqrt{(1-x^2)(1-y^2)} \sin \chi). \quad (78)
 \end{aligned}$$

In new variables (75)-(77) the equation for scattering rate (72) is

$$\begin{aligned}
 R_{ee} &= \frac{1}{I+1} \frac{g_e^2}{2^{11} \pi^6} \int_{2m}^{\infty} dq_0 \exp(q_0) \int_0^1 dz z^2 (q_0^2 - 4m^2)^{3/2} \int_0^{2\pi} d\chi \int_{-1}^1 dx \int_{-1}^1 dy \left(1 - \frac{4m^2}{s}\right) f_e \left(\frac{q_0}{2} + p_0\right) \Upsilon_e^{-4} \\
 &\quad \times \sum |M_{ee}|^2 f_e \left(\frac{q_0}{2} - p_0\right) f_e \left(\frac{q_0}{2} + p'_0\right) f_e \left(\frac{q_0}{2} - p'_0\right). \quad (79)
 \end{aligned}$$

TABLE II: Values of N and A for the power law temperature dependence of thermal cross section high energy tail, see Eq.(34) for the shape assumed, for cross sections presented in figure 6.

Reaction	N	A [mb]
$\gamma e \leftrightarrow \gamma e$	-1.73	120
$\gamma\gamma \leftrightarrow e^+e^-$	-1.73	80
$e^+e^- \leftrightarrow \gamma\gamma$	-1.73	46

IV. NUMERICAL RESULTS AND DISCUSSION

A. Thermal cross section and Thompson limit

The thermally averaged cross sections $\langle v\sigma \rangle / c$ in observer frames for pair production, annihilation and Compton scattering Eq.(4), (5) are evaluated using the Lorentz-invariant rates, Eq.(20) with rates, evaluated numerically using Eq.(51) for pair production and annihilation and Eq.(66) for Compton scattering. In Fig. 6 we show $\langle v\sigma \rangle / c$ for Compton scattering (dashed red line), pair production (solid blue line) and pair annihilation (dash-dotted green line). For high T we observe the power law fall-off of the thermal cross sections and the corresponding parameters are presented in Table II. The power $N = 1.73$ in power law for pair production/annihilation and Compton scattering is close for nonthermal cross section in this case. At high temperatures these cross sections are almost parallel. This is in agreement with t -averaged cross sections Eqs.(31)-(32).

Considering electron production, the density of photons with energy larger than the threshold for pair production drops in the tail of Boltzmann distribution with decreasing temperature, therefore the thermal cross sec-

tion $\langle v\sigma \rangle$ starts to decrease at $T < m$ and goes to 0 as $T \rightarrow 0$. For electron-positron annihilation $\langle v\sigma \rangle / c$ stays for $T \rightarrow 0$, $v \rightarrow 0$, since $\sigma \propto 1/v$.

At $T \ll m$, the Compton scattering cross section $\langle v\sigma \rangle$ is approaching the Thompson limit very slowly, which in case $\Upsilon = 1$ is slightly $[\langle v\sigma \rangle_{comp} (\Upsilon = 1) / c\sigma_{th} \approx 1.36]$ above the actual classical Thompson cross section

$$\sigma = \frac{8\pi\alpha^2}{3m^2} = 6.7 \times 10^2 \text{ mb}.$$

This result is shown in Fig. 7 (dashed red line). This difference with the Thompson limit is due to quantum effects from massless photons. We can use Boltzmann distribution for photons only when $\Upsilon_\gamma \ll 1$. In this case we obtain that thermal Compton cross section goes to the Thompson limit (green solid line in Fig. 7). In order to explain the difference between the cross section for $\Upsilon_\gamma = 1$ and the Thompson limit, we assume that electrons are at rest at small T and thermal photons are scattering without energy change $E_i = E_f$. Then the cross section quantum enhancement factor Q is the thermal average from the Bose enhancement factor $f_\gamma(p) + 1$:

$$Q = \frac{g_\gamma}{2\pi^2 n_\gamma} \int_0^\infty f(p)(f(p) + 1)p^2 dp. \quad (80)$$

In the Boltzmann limit $f(p) + 1 \rightarrow 1$ and $Q \rightarrow 1$. For $\Upsilon_\gamma = 1$ we obtained $Q = 1.38$. Further discussion about the Boltzmann and the quantum limit comparison is found in Sec. IV C

B. Mean Free Paths

In Fig. 8 (left panel) we show the mean free paths of electron (positron) in EP³ plasma in pair annihilation

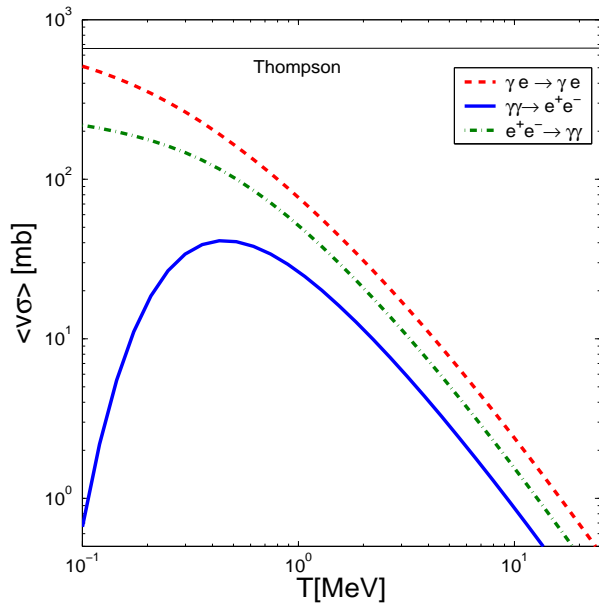


FIG. 6: The thermally averaged cross sections $\langle v\sigma \rangle/c$ for Compton scattering (dashed red line), pair production (solid blue line) and annihilation (dash-dotted green line) in the observer rest frame shown as a function of temperature T at $\Upsilon = 1$

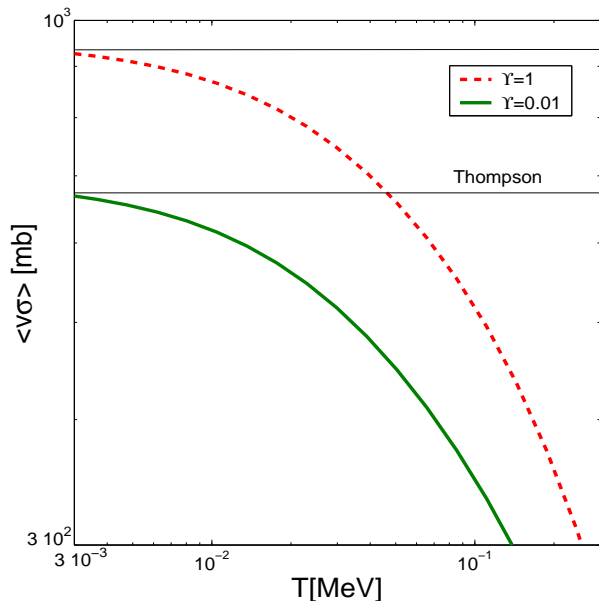


FIG. 7: The thermally averaged cross sections $\langle v\sigma \rangle/c$ for Compton scattering for $\Upsilon_\gamma = 1$ (dashed red line) and $\Upsilon_\gamma = 0.01$ (solid green line) as a function of temperature T .

and Compton scattering reactions Eqs.(4) and (5) (green dash-dotted and red dashed lines, respectively), and in Møller and Bhabha scattering reactions Eqs.(6) and (7) together (purple solid line) ($\Upsilon_e = \Upsilon_\gamma = \Upsilon = 1$). The

mean free paths are evaluated according to Eq.(21):

$$L_{ee \rightarrow \gamma\gamma} = \frac{n_e}{R_{ee \rightarrow \gamma\gamma}}; \quad L_{e\gamma} = \frac{n_e}{R_{e\gamma}}; \quad L_{ee \rightarrow ee} = \frac{n_e}{R_{ee}}$$

with rates evaluated, using Eq.(51) for pair annihilation, Eq.(66) for Compton scattering, and Eq.(79) for Møller and Bhabha scatterings. To determine the possible radius of opaque and equilibrated plasma [equivalent to opaqueness condition, Eq. (2), being satisfied] at a given energy, we show the radius of a plasma drop as a function of temperature [using Eq.(11)] at expected experimental energies 500 J (upper light blue dotted line) and 50 J (lower purple dotted line).

The mean free path of electron or positron in Møller and Bhabha scattering remains much below the equilibrium plasma radius at energy 500 J and the temperature range considered here, up to the smallest temperature considered $T \cong 0.3$ MeV. Therefore electrons and positrons are thermally equilibrated at our temperature range. The L_e in Møller and Bhabha scattering is much smaller than L_e in Compton scattering and in pair annihilation. Therefore electron and positron become thermally equilibrated first after their production by the laser field and then they produce photons over the larger time scale.

We do not continue calculations for smaller temperatures since for ($T \ll m_e$) it becomes impossible to create equilibrium plasma with zero chemical potential considered here, and hence for this reason our calculations of Møller and Bhabha scattering rates are developed for temperatures $T \gg m$.

In Fig. 8 (right panel) the mean free photon paths L_γ are shown for e^+e^- pair production reaction (solid blue line) and Compton scattering (dashed red line) as functions of temperature T for plasma in chemical equilibrium ($\Upsilon_i = 1$). Equation (21) is used together with Eqs. (51) and (66) for pair production and Compton scattering rates:

$$L_{\gamma\gamma \rightarrow ee} = \frac{n_\gamma}{R_{ee \rightarrow \gamma\gamma}}; \quad L_{\gamma e} = \frac{n_\gamma}{R_{e\gamma}}.$$

The mean free paths for photon and electron scattering presented in Fig. 8 have power law distribution at high temperature, $T \gg m$,

$$L = A \left(\frac{T}{1 \text{ MeV}} \right)^N. \quad (81)$$

The coefficients A and N for mean free paths are listed in Table III.

We see that $L_{\gamma e}$ is less than $L_{\gamma\gamma}$ at $\Upsilon = 1$ over the full range of temperatures considered. The line for $L_{\gamma e}$ follows that for $L_{\gamma\gamma}$ at $T > m_e$ and $L_{\gamma e}$ is about 4 times smaller than $L_{\gamma\gamma}$, when values of $L_{e\gamma}$ are about twice as low as $L_{ee \rightarrow \gamma\gamma}$ at high temperatures. The factor making $L_{\gamma e}$ to be half the length $L_{e\gamma}$ is the photons scattering on both electrons and positrons.

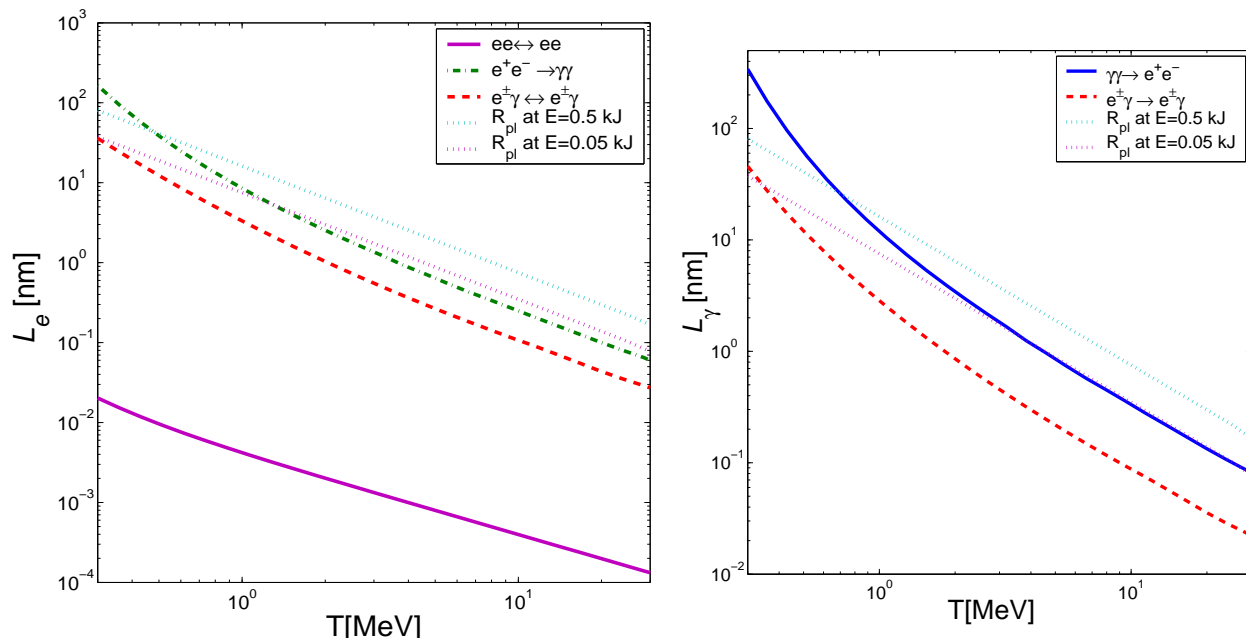


FIG. 8: Left panel: the mean free paths of electron (positron) shown as functions of plasma temperature in reactions Eqs.(4), (5)(red dashed, green dash-dot lines, respectively), and reactions Eqs.(6) and (7) together (purple solid line); right panel: the mean free path of photon for Compton scattering and pair production at $\Upsilon = 1$ (red dashed and blue solid lines) as functions of temperature T ; radius of equilibrium ($\Upsilon = 1$) plasma at energy 500 J (upper, light blue, dotted line) and at energy 50 J (lower, purple, dotted line) as a function of T on both sides.

TABLE III: The values of N and A in the power law temperature dependence of free mean path high energy tail, Eq.(81)

reaction	N	A [nm]
$L_\gamma, \gamma e \leftrightarrow \gamma e$	- 1.3	1.8
$L_\gamma, \gamma\gamma \leftrightarrow e^+e^-$	-1.3	6.5
$L_e, \gamma e \leftrightarrow \gamma e$	- 1.3	5
$L_e, e^+e^- \leftrightarrow \gamma\gamma$	- 1.3	2
$L_e, ee \leftrightarrow ee$	- 1	0.004

At small temperatures, $T \leq m$, the photon mean free path L_γ drops with temperature faster than the plasma radius at a fixed energy. Plasma loses opaqueness when $L_{\gamma e}$ approaches the plasma radius in magnitude. For $T \approx 0.5$ MeV the free photon path $L_{\gamma e}$ is much smaller than radius of plasma, $R = 35$ nm, at energy 500 J. Since plasma is opaque, photons will stay in plasma volume for a long time. For $T < 0.5$ MeV plasma becomes nonopaque and can lose energy, radiating photons. The plasma, which is opaque for photons, cannot have a radius larger than $R \approx 35$ nm for the considered energy content. In Table IV we show the values of maximum radius, minimum temperature and corresponding e^+e^- pair and photon densities for opaque plasma at fixed energies 500 and 50 J.

Because at high temperatures the mean free paths decrease slower than the plasma radius, $R \propto T^{4/3}$. Therefore there is a limit on the minimum energy need to create opaque plasma. A similar energy limit also exists for

TABLE IV: The values of maximum radius, minimum temperature and corresponding e^+e^- pair and photon densities for opaque plasma at fixed energies 500 and 50 J

E [J]	opaque R_{max} [nm]	opaque T [MeV]	opaque n_γ [cm^{-3}]	opaque n_e [cm^{-3}]
500	35	0.5	3.9×10^{30}	5×10^{30}
50	3	2	2.55×10^{32}	3.8×10^{32}

chemically equilibrated plasma, condition Eq.(3). The energy $E = 500J$ is not large enough to satisfy this equilibration condition exactly, but it is close to the minimum of required energy. The largest ratio $R/L_{\gamma\gamma} \approx 2$ arises at temperatures $T \approx 4 - 6$ MeV (Fig. 8, right panel) and plasma may be close to chemical equilibrium at this temperature range. The corresponding radius is ≈ 2 nm. The pair production or annihilation relaxation time Eq. (16) is approximately 10^{-3} fs at $T = 5$ MeV and the corresponding plasma lifespan must be larger than that to satisfy the chemical equilibration condition.

In this work we considered the highest density of chemical equilibrium plasma at $\Upsilon_e = \Upsilon_\gamma = \Upsilon = 1$ (for photon opaqueness condition $\Upsilon_e = 1$ is enough), because the opaqueness condition Eq.(2) is quickly violated with Υ_i decreases. This is because the photon free path $L_\gamma \propto 1/\Upsilon$, when the radius of plasma $R_{pl} \propto 1/\Upsilon^{1/3}$, Eq.(12). The result is $R_{pl}/L_\gamma \propto \Upsilon^{2/3}$ at a fixed energy content. Only for the relatively high plasma temperature

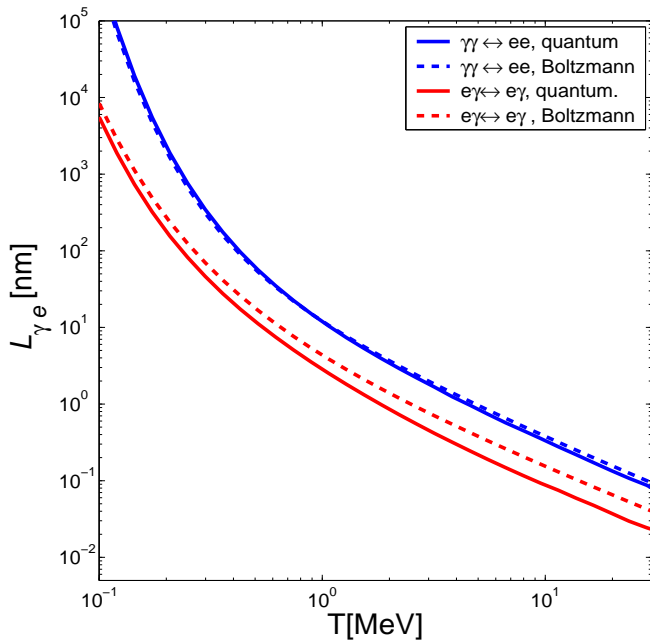


FIG. 9: The photon mean free path for Compton scattering (lower red lines) and pair production (upper blue lines) obtained using reaction rate Eq.(66) (solid lines) and using rate from Eq.(82)(dashed lines), Boltzmann limit

is it possible to have a below equilibrium density plasma with small Υ , without violation of opaqueness condition Eq.(2). For example at $T = 20$ MeV and energy 500 J $R_{\text{pl}}/L_{\gamma e} \approx 8$. In this case minimum possible $\Upsilon \approx 0.3$ and radius at fixed plasma energy increases by factor of ≈ 1.4 only (≈ 0.4 nm), as the result $R_{\text{pl}}/L_{\gamma e} \approx 3$.

C. Lorentz-invariant rates and Boltzmann limit

In order to evaluate the reaction rate in two - body processes in the relativistic Boltzmann (classical) limit, we can use reaction cross section $\sigma(s)$, and the relation [17]:

$$R_{12 \rightarrow 34} = \frac{g_1 g_2}{32\pi^4} \frac{T}{1+I} \int_{s_{th}}^{\infty} ds \sigma(s) \frac{\lambda_2(s)}{\sqrt{s}} K_1(\sqrt{s}/T), \quad (82)$$

(however, compared to Ref. [17] Eq.(17.16) $R_{12 \rightarrow 34} \rightarrow R_{12 \rightarrow 34}/(\Upsilon_1 \Upsilon_2)$), where

$$\lambda_2(s) = (s - (m_1 + m_2)^2)(s - (m_1 - m_2)^2), \quad (83)$$

m_1 and m_2 , g_1 and g_2 , Υ_1 and Υ_2 are masses, degeneracy and fugacities of initial interacting particles.

The cross sections can be evaluated using Eq. (31)-(33). In cases considered here Eq. (82) with t-averaged cross section gives the same result for reaction rate as Eq.(22) with $\Upsilon \rightarrow 0$. In the general case the cross section averaging over t may also change the result compared to Eq. (22). Calculating mean free path L in the Boltzmann limit we also took the photon density in the Boltzmann

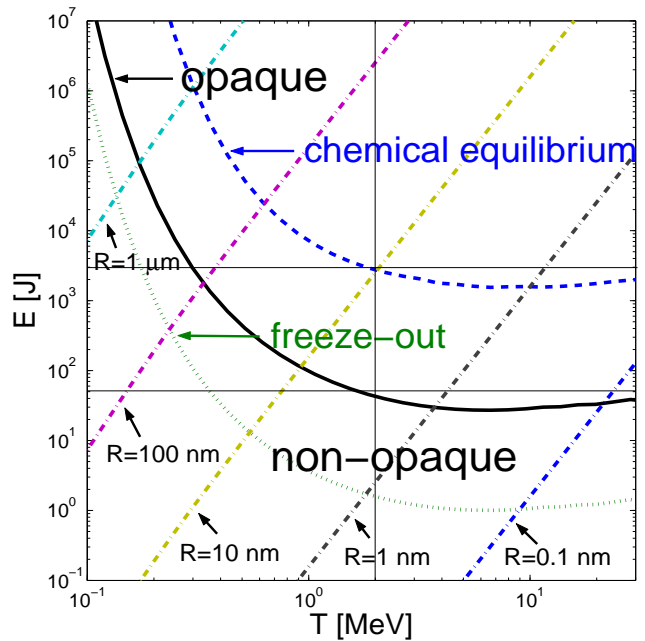


FIG. 10: The energies of plasma drop with different radius ($R = 1\mu\text{m}$, 100 nm, 10 nm, 1 nm and 0.1 nm) as a functions of T (dash-dotted lines - light blue, purple, brown, grey and blue, respectively); solid black line is energy vs. minimum T of opaque plasma; dashed blue line is energy vs. minimum T of chemically equilibrated plasma;)

limit as $n_\gamma \rightarrow n_\gamma/\Upsilon$ at $\Upsilon \rightarrow 0$ to exclude all quantum distribution effects.

In Fig. 9 we show our mean free paths for a photon subject to Compton or pair production process, for both quantum and Boltzmann (classical) limit as a functions of T . For Compton scattering quantum effects reduce the mean free path at high density (i.e. high T). Somewhat smaller, but a noticeable quantum effect remains at low temperature ($T < m$). For pair production there is no reduction of the mean free path at small temperature because of the threshold energy of photons in the pair production rate, and the smaller reduction for high T compared to Compton scattering.

V. SUMMARY AND CONCLUSION

Current laser pulses can have energies up to 1 kJ and about 10 kJ is expected to be produced in the foreseeable future [16]. Since we need to focus energy to sub diffraction size limit, $R \ll \lambda$, only a part of the original energy is likely to be available to form plasma.

The main purpose of this paper has been the evaluation of the domain of plasma size and temperature where thermally and chemically equilibrated EP³ can exist at a given fireball energy. We evaluate the mean free path length L for photons and electrons in EP³ plasma, assuming thermal equilibrium and using the Lorentz invariant reaction rate. This method allows us to take into account

quantum effects in a dense medium.

Comparison of the electron (positron) mean free path with the plasma radius (figure 8, left) demonstrated that electrons and positrons can be thermally equilibrated by Møller and Bhabha scattering at the temperature range that we considered. The small free path of electron and positron by Møller and Bhabha scattering, compared to e^+e^- pair annihilation, also means that electrons and positrons first become thermally equilibrated and then they produce thermal photons.

Comparison of photon mean free path L_γ to plasma drop size R_{pl} (see figure 8, right) indicates that we may have restrictions on maximum plasma size, minimum temperature and minimum energy of opaque and chemically equilibrated plasma, defined by opaqueness condition Eq.(2). We find that the mean free path for γe Compton scattering is shorter than for pair production $\gamma\gamma \rightarrow e^+e^-$. Therefore opaqueness condition for photon will have $L_\gamma = L_{\gamma e \leftrightarrow \gamma e}$ and differs from chemical equilibration condition Eq.(3).

The practical summary of our results is presented in figure 10. The energies of different size plasma drops are shown as a function of temperature. The solid black line indicates the boundary below which the opaque plasma cannot exist; condition Eq.(2) is violated. The blue dashed line indicates the boundary above which we have not only opaque but also chemically equilibrated plasma, condition Eq.(3). The green dotted line shows photon chemical freeze-out, $L_\gamma/R_{pl} = 1$. The straight lines show constraints given by plasma size between E and T .

In Fig. 10 we see that at fixed plasma size to have opaque plasma less energy is needed than to have chemically equilibrated plasma; for fixed energy the transition to chemically equilibrated plasma takes place at a smaller plasma sizes and higher temperatures and energies than the transition to opaque plasma.

Only for $E > 50$ J can we expect to form an opaque plasma for $T > 2$ MeV. As more energy becomes available, the temperature limit drops and the radius increases ($R > 5$ nm). It is interesting to note that much more energy is needed to produce opaque plasma at lower compared to higher temperature, because plasma drop size has to increase considerably to satisfy the opaqueness condition Eq(2). Thus one of main objectives of laboratory experiments should be to seek paths to reduce the size of the domain in which energy deposition occurs.

To summarize, our results indicate that chemically equilibrated, opaque, small – size is about 5-50 nm – plasma drop can be formed for energy of a few kJ which may be experimentally attainable in foreseeable future. Such a plasma drop would be an extraordinarily intense source of radiation and positrons.

Acknowledgments

This work was supported by the DFG Cluster of Excellence MAP (Munich Centre of Advanced Photonics), and by a grant from: the U.S. Department of Energy DE-FG02-04ER41318.

-
- [1] I. Kuznetsova, D. Habs and J. Rafelski, Phys. Rev. D **78**, 014027 (2008)
 - [2] G. A. Mourou, T. Tajima and S. V. Bulanov, Rev. Mod. Phys. **78**, 309 (2006).
 - [3] M. Marklund and P. K. Shukla, Rev. Mod. Phys. **78**, 591 (2006) [arXiv:hep-ph/0602123].
 - [4] R. Ruffini, G. Vereshchagin and S. S. Xue, Phys. Rept. **487**, 1 (2010) [arXiv:0910.0974 [astro-ph.HE]].
 - [5] P. Koch, B. Muller and J. Rafelski, Phys. Rept. **142**, 167 (1986).
 - [6] T. Matsui, B. Svetitsky and L. D. McLerran, Phys. Rev. D **34**, 783 (1986) [Erratum-ibid. D **37**, 844 (1988)].
 - [7] T. Weaver Phys. Rev. A , **13**, 1563 (1976)
 - [8] R. Svensson, Astrophys. J. **258**, 321 (1982).
 - [9] J. Letessier, J. Rafelski and A. Tounsi, Phys. Rev. C **50**, 406 (1994).
 - [10] B. L. Combridge, Nucl. Phys. B **151**, 429 (1979).
 - [11] J.M.Jauch and F.Rohrlich "The theory of photons and electrons", Texts and Monographs in physics, Springer-Verlag, 1976
 - [12] A. G. Aksenov, R. Ruffini and G. V. Vereshchagin, Phys. Rev. D **79**, 043008 (2009) [arXiv:0901.4837 [astro-ph.HE]].
 - [13] F. Halzen and A. D. Martin, "Quarks And Leptons: An Introductory Course In Modern Particle Physics," *New York, Usa: Wiley (1984) 396p*
 - [14] T. S. Biro, P. Levai and B. Muller, Phys. Rev. D **42**, 3078 (1990).
 - [15] Markus H. Thoma, Rev. Mod. Phys.**81**, 959 (2009).
 - [16] Ed Gerstner, Nature **446**, 16, (28 February 2007) doi:10.1038/446016a
 - [17] J. Letessier and J. Rafelski, Camb. Monogr. Part. Phys. Nucl. Phys. Cosmol. **18**, 1 (2002).